WORLD CONFERENCE ON TIMBER ENGINEERING 2025
BRISBANE, AUSTRALIA
Advancing Timber for the Future Built Environment

MECHANICAL PERFORMANCE ANALYSIS OF CLT AND STRUCTURAL TIMBER RAILS UNDER COMPRESSION TESTS

Marcus Vinicius Tavares da Costa[1], Loïc Vieilledent[2], Mikael Perstorper[3], Johan Vessby[4]

ABSTRACT: Prefabricated timber modules can help make the building sector more sustainable by reducing greenhouse gas emissions. However, structural challenges, like vertical relative deformations and the buckling of timber studs on timber rails still limit the height of tall timber buildings. These challenges are affected by how studs and rails interact. This study aims therefore to investigate this interaction by experimental tests and finite element (FE) modelling of five-layer Cross Laminated Timber and structural timber bottom rails under compression loads applied perpendicular to the rails via structural timber studs. Results from the conceptual compression tests with centric and eccentric loads show that CLT bottom rails have a much higher loading-bearing capacity compared to structural timber bottom rail. Additionally, local penetrations were observed in the contact zone between stud and rail which were included in the FE models allowing to estimate the contact stiffness.

KEYWORDS: Cross laminated timber rails, Structural timber rails, Compression test, FE modelling

1 – INTRODUCTION

In order to reduce the environmental impact of the building industry, timber structures are now in focus and their use is expected to grow in the sector in the coming years. The increased use of structural timber in tall buildings is one example [1]. However, there are still several challenges in the design of tall timber structures, in particular global vertical relative deformations of the structures. A new idea to reduce these deformations is to make rails from CLT cut-offs for which the cross layers substantially enhance the load bearing capacity under compression [2]. Repurposing the waste cut-outs is also economically and environmentally beneficial. In this context, the new CLT rails needs to be further examined, in particular the interaction between structural timber studs and rails under high compressive loads.

The purpose of this study is therefore to investigate experimentally and numerically the stiffness and strength of CLT and their class equivalent, structural timber C24, bottom rails during compression loading by timber studs. In the presented study, the customized tests coupled with digital image correlation (DIC) also explore loading eccentricity to induce rotation on the studs for mimicking potential buckling case around the strong axis of studs in the bottom floor of tall timber buildings. A stiffer CLT-based rail might increase the buckling load by working as a partially fixed end if supported by concrete or the like. Finite element (FE) models were developed and calibrated with the tests to understand the mechanical contributions of different zones in the stud-rail systems with the primary focus on the contact behaviour. The main objective of this study is to mechanically analyze stud-rail interactions to develop simplified structural elements for scaling up models.

2 – MATERIALS AND METHODS

2.1 MATERIALS

In this study, two five-layer CLT boards with different width were supplied (Stora Enso Mill, Gruvön, Sweden) made of Norway spruce were used in the compression

[1] Marcus Vinícius Tavares da Costa, Karlstad University, Sweden, marcus.tavares@kau.se, ORCID ID: 0000-0002-0491-1077

[2] Loïc Vieilledent, Karlstad University Sweden and Supmicrotech ENSMM France, loicvieilledent@gmail.com

[3] Mikael Perstorper, Karlstad University and Dynalyse AB, Sweden, mikael.perstorper@kau.se

[4] Johan Vessby, Karlstad University, Sweden, johan.vessby@kau.se, ORCID ID: 0000-0003-1638-1023

https://doi.org/10.52202/080513-0606

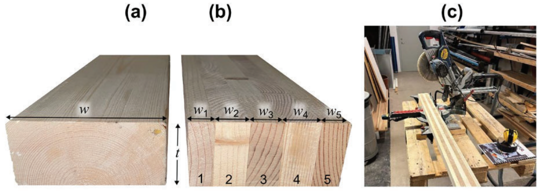

***Figure 1**: (a) C24 board, (b) CLT board and (c) cutting the boards.*

tests. The boards were strength graded as a single grade to T15 were produced by REX laminations from cut-offs of the CLT production [2, 3]. One board had a cross sectional area (t × w) of 45 × 95 mm^2 while the other measured 45 × 170 mm^2.

Fig. 1(b) shows a photograph of the 95-mm wide CLT board, for which the layers 1,3 and 5 are the 0° layers with widths of w_1=w_5=17 mm and w_3=20.3 mm and the layers 2 and 4 are 90° layers both with widths of w_2=w_4=20.3 mm.

The wider CLT board of 170 mm had the same configuration, but with layers widths of w_1=w_5=40 mm and w_2=w_3=w_4=30 mm instead. The studs, see Fig 1(a), were cut from C24 boards with the same cross-sectional area as the corresponding CLT boards.

For the rails, a planer (Robland NX310, Belgian) was used to guarantee parallelism between top and bottom surfaces. The thicknesses of the rails t were planed to a cross-section dimension of 40 × 95 mm^2 and 40 × 170 mm^2 to secure this. Then, 24 pieces of 300 mm long rails were cut from the planed boards by using a circular saw (Bosch GCM8SJ, Germany) as shown in Fig. 1(c). From each board, including the C24 boards, 6 testing rails were produced.

For the studs, the C24 boards were cut in pieces of 210 mm length, but without planing. Before the tests, all rails and studs were conditioned for at least 48 hours in a standard climate to achieve a moisture content of 12% for the timber materials [4]. The measured average value for the density were 491 kg/m^3 for CLT and 421 kg/m^3 for C24 materials.

2.2 COMPRESSION TESTS

The experiments shown in Fig. 2(a-d) were carried out in a hydraulic press (MEGA 6-3000-200, Form+test Prüfsysteme, Germany). The load was applied in a crosshead displacement control mode with a loading rate of 2 mm/min while sampling the force F. At the top of the stud, a steel roller was positioned between two steel plates where the plate 1 was attached to the crosshead with no rotations while the plate 2 was placed on the top of the studs. This was made to enable horizontal displacements when the roller is not positioned in the centre line of the stud.

In this experimental configuration, three centric and three eccentric tests for each of the two widths were carried out for rails of structural timber class C24 and likewise for rails of CLT. The eccentric tests had the roller horizontally shifted from the centre line e = 20 mm for the 95-mm wide rails and e = 30 mm for the 170-mm wide rails. For all tests the rail was loaded in the centre of the 300 mm total length. A DIC method using a stereo-camera system (Aramis-GOM, Germany) was used to measure displacements from DIC markers at the steel plates positioned on the stud and at the stud. The five DIC markers on the studs were located 50 mm above the top surface of the rail and horizontally located in the middle of each layer in the CLT-board.

3 – FINITE ELEMENT MODEL

Using the FE software Abaqus, two models were developed with the same dimensions as in the tests: One with a rail of C24 and another with a rail of CLT. Fig. 3(a) shows the assembly of the models. A vertical and horizontal displacements v and u were applied to the reference point of the plate 2 while the displacement along z- axis were prescribed to zero. The displacements were v = 4 mm and u = 0 for the centric cases and v = 4 mm and the function

$$u = \begin{cases} 0, & v < v_e \\ a(v_e - v), & v > v_e \end{cases} \tag{1}$$

for the eccentric cases where a is slope parameter and v_e is the coupled displacements onset. The function was adjusted based on the DIC targets in the plate 2 with the experiments. To allow the in-plane tilting of the stud, the rotations along x- and y-axis were zero while the one along z-axis was free. Tie constrains were used between the plate 2 and the stud on top. In this region, the studs were partitioned to create a first “damage zone” (dz1) with reduced stiffness. Damage zones occurs in low compressive stresses between wood parallel to the grain to steel plates caused by difference in surface roughness [5]. When the surfaces are pushed into each other, the uneven contact causes bending/buckling of the fibres leading to a lower effective stiffness in this zone [6]. The size and stiffness of damage zones were determined in Appendix A.2.

https://doi.org/10.52202/080513-0606

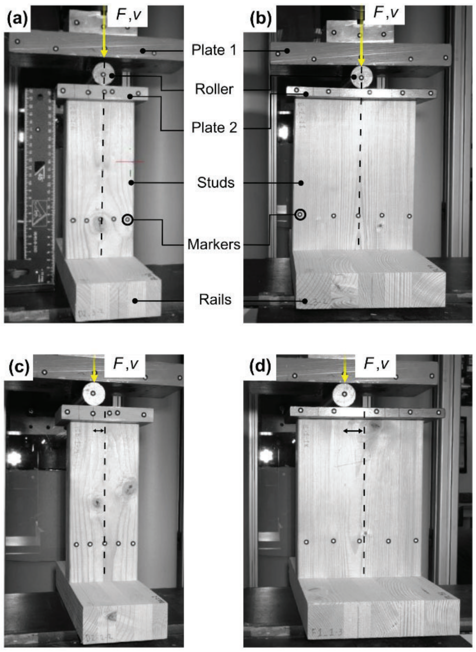

Figure 2: Centric experimental setups of (a) the 95-mm wide and (b) the 170-mm wide configurations. Similarly, eccentric experimental setups of (c) the 95-mm wide and (d) the 170-mm wide configurations.

Contact conditions were used between studs and rails where the tangential behaviour was modelled with a friction coefficient of 0.4 [7] and the normal behaviour was linear pressure-overclosure. Pressure-overclosure contacts are computationally efficient alternative for handling complex penetration problems where the contact pressure governs the overclosure of the surface meshing as shown in the right-hand side in Fig. 3(a). In this study, linear behavior in the overclosuring interactions was assumed with two different normal contact stiffnesses K_{contact}, for 0°/90° wood contact (layers 0,1,3 and 5) and 0°/0° wood contact (layers 2 and 4). These stiffnesses were calibrated with the tests.

In the bottom surface of the rails, full interaction was assumed with the substrate and a second "damage zones" (dz2) was used, see also Appendix A.2. For meshing, 20-node quadratic brick elements (C3D20) of 5 mm size were used as illustrated in Fig. 3(b).

The plate 2 is simply modelled as a rigid element. The wood parts are orthotropic elastic-plastic where cylindrical coordinate systems were assigned to each part to reproduce wood material orientations (*L*=longitudinal, *R*=radial and *T*=tangential). The local systems have their origins at the pith locations P_0 for the C24 rails and studs and $P_{1\text{-}5}$ for each layer of the CLT rails (see Fig. 3 (c)

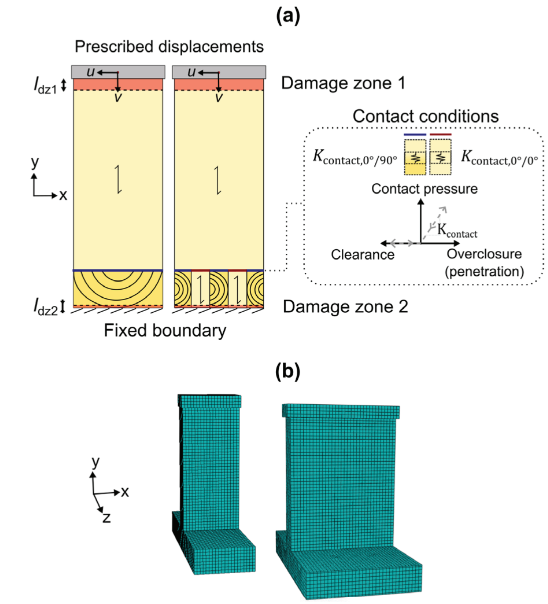

(c)

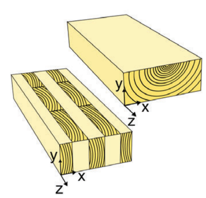

Pith index	Pith Location	
	95-mm wide rails	170-mm wide rails
P_0	(47.5, 40, z)	(85, 40, z)
P_1	(-40, 20, z)	(-40, 20, z)
P_2	(-23, y, 50[1-2×n])	(-26, y, 50[1-2×n])
P_3	(2, 20, z)	(30, 20, z)
P_4	(18, y, 50[1-2×n])	(60, y, 50[1-2×n])
P_5	(135, 20, z)	(210, 20, z)

Figure 3: (a) The FE models with their boundary conditions and (b) meshing. (c) The pith locations of the CLT and C24 materials in the models.

where the reference is the cartesian coordinate system at the bottom left corner of each material). The CLT layers 2 and 4 are subdivided in *n* periodic layers with their lengths and distances between their piths of 100 mm along the z-axis.

The Abaqus built-in Hill plasticity model was applied to the wood materials with initial compressive yield stresses determined based in the values reported in [8]. Isotropic hardening functions parallel and perpendicular to the grains were chosen with two tabulated points for the reference stresses vs. plastic strains. The trends of the data points are typical for wood and are consistent with the compressive stress-strain curves, e.g., in [5, 8]. Some elastic properties of the wood material used were measured, see Appendix A.1, and others were estimated from previous studies [5, 8, 9]. Material parameters used are given in Table 1.

4 – EXPERIMENTAL RESULTS

4.1 FORCE vs. DISPLACEMENT

The global deformation of the stud-rail set-up versus load is show in Fig. 4. The stiffness of 95-mm wide CLT bottom rails (155 kN/mm) were three times as high than of 95-mm wide C24 timber rails (52 kN/mm). The stiffnesses were determined from the initial linear portion of the average curves in the force range of F = 20-50 kN for CLT and F = 8-18 kN for C24 rails. The average maximum force $F_{\max.CLT.95}$ was 87 kN for CLT rails and $F_{\max.C24.95}$ = 37 kN at v = 4 mm for C24 rails.

The stiffness of 170-mm wide CLT bottom rails (260 kN/mm) were four times higher than that of C24 timber rails (62 kN/mm). The stiffnesses were determined from the initial linear portion of the average curves in the force range of F = 50-90 kN for CLT and F = 14-22 kN for C24 rails. The average maximum force was $F_{\max.CLT.170}$ =148 kN for CLT rails and $F_{\max.C24.170}$ = 57 kN at v = 4 mm for C24 rails.

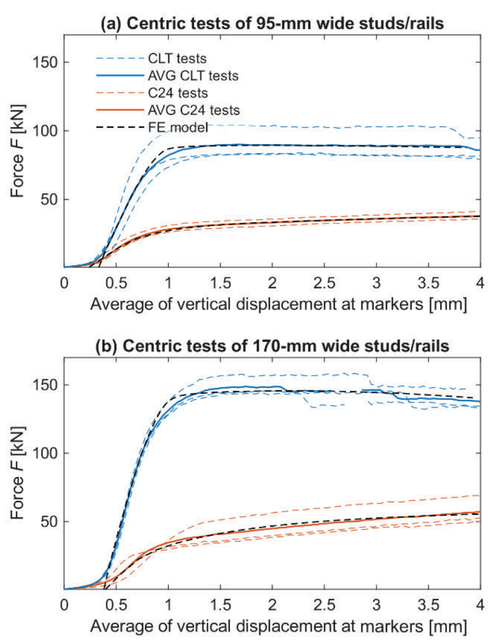

***Figure 4**: Force F (load cell) as a function of average vertical displacement at DIC markers from the centric tests for (a) the 95-wide and (b) the 170-wide configurations.*

***Table 1**: Mechanical properties of wood used in the FE models.*

Elastic constants Rails/Studs [MPa] [8 ,9]		**Initial compressive yield stresses [MPa]** [5, 8, 9]	
E_R **[MPa]**	1100/1100*	σ_R **[MPa]**	4.0 ± 1.0
E_T **[MPa]**	730/730*	σ_T **[MPa]**	4.0 ± 1.0
E_L **[MPa]**	17326/11120*	σ_L **[MPa]**	42.0 ± 3.0
ν_{RT} **[-]**	0.3/0.3	σ_{RT} **[MPa]**	2.3 ± 0.2
ν_{RL} **[-]**	0.02/0.02	σ_{RL} **[MPa]**	4.5 ± 0.5
ν_{TL} **[-]**	0.020.02	σ_{TL} **[MPa]**	4.5 ± 0.5
G_{RT} **[MPa]**	50/50		
G_{RL} **[MPa]**	747/895*		
G_{TL} **[MPa]**	747/895*		
Reference yield stresses vs plastic strains			
Reference yield stresses σ_0		**Plastic strain** ε_p	
		$\varepsilon_p = 0$	$\varepsilon_p = 0.4$
$\sigma_0 = \sigma_L$ **(Parallel to the grains)**		42.0 ± 3	38.0 ± 3.0
$\sigma_0 = \sigma_{R,T}$ **(Perpendicular to the grains)**		4.0 ± 0.5	6.0 ± 1.0

*Mean values measured from dynamic modal tests in Appendix A.1.

4.2 FORCE vs. ROTATION

In the setups with initial eccentricity, the measured relationship between force F and rotation α at the markers on the studs is shown in Fig. 5. The following results are based on the average of only three tests and should therefore be interpreted with caution. According to Eurocode the design axial compression strength for a C24 stud with cross-section dimensions 45×95 mm and a length of 3 m is $N_{\mathrm{Rd.95}}$ = 14.3 kN while buckling around the weak axis is prevented and no loads causing flexure of the member are applied. At this load the observed rotation was $\alpha_{\mathrm{C24}} = 4.4 \cdot 10^{-3}$ rad for the tested stud, while for the CLT rail, it was $\alpha_{\mathrm{CLT}} = 1.5 \cdot 10^{-3}$ rad. This corresponds to a 3 times larger rotation in the structural timber (C24) rail compared to the CLT rail.

The corresponding buckling design strength for the stud with the width of 170 mm can be calculated similarly to $N_{Rd.170}$ = 65.5 kN. However, experimental data are not available at such high loads so the rotations has instead been taken at F = 50 kN. The observed rotation at this and other loads are presented in Table 2 to facilitate comparison between the two widths and to better understand of the difference in stiffness. It should be noted that the initial eccentricity, e_{init}, varies between the two widths, so a direct comparison between them is not possible. This also implies that the moment at various load stages, $M_i = F_i \cdot e_{tot}$, causing the rotation will be different at for different rail materials at the same forces F_i. Results are presented in Table 2 and shows that the

https://doi.org/10.52202/080513-0606

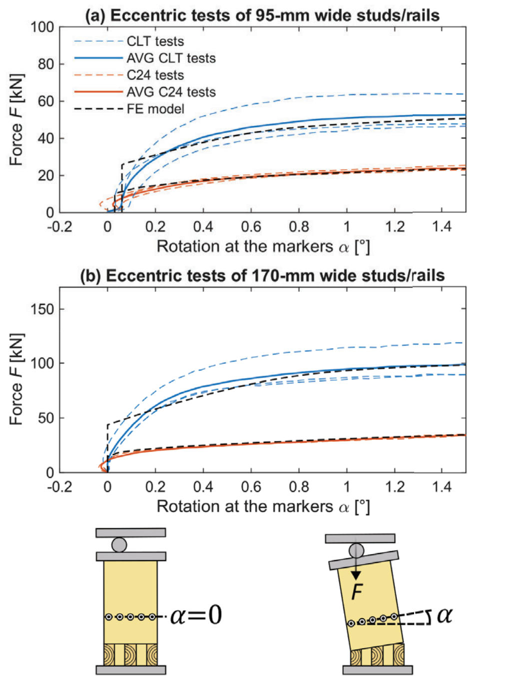

Figure 5: Force F (load cell) as a function of rotation at DIC markers from eccentric tests for (a) the 95-wide configuration and (b) 170-mm wide configuration.

rotational stiffness in CLT is significantly higher than in structural timber caused by the stiff layers 2 and 4. This means that a CLT-rail may increase the buckling load of a stud in the strong direction since it will work as a partly fixed end.

For both stud widths and rail types the displacement used by the vertical load, F_i, and the moment caused by the eccentricity, $M_i = F_i \cdot e_{tot}$, are plotted in Fig. 6. The

Table 2: Observed rotations in the eccentric tests for different load levels. Note that closest fit to force is used.

Width	w = 95 mm, angle $\alpha \cdot$ 1000, M [kNm]			w =170 mm, angle $\alpha \cdot$ 1000, M [kNm]		
***Rot*@ *F*[kN] / and *M*[kNm]**	**C24**	**CLT**	**C24/ CLT [-]**	**C24**	**CLT**	**C24/ CLT [-]**
***Rot*@ F_1=10**	2.1	1.2	1.8	-	-	-
$F_1 \cdot e_{tot}$	0.21	0.20	1.0	-	-	-
***Rot*@ F_2=14.3**	4.4	1.5	3.0	0.72	0.12	6.2
$F_2 \cdot e_{tot}$	0.29	0.29	0.98	0.43	0.43	1.0
***Rot*@ F_3=20**	11.8	2.0	5.9	3.6	0.38	9.4
$F_3 \cdot e_{tot}$	0.42	0.40	1.0	1.08	0.62	1.7
***Rot*@ F_4=30**	102	3.9	26.4	17.5	1.1	16.6
$F_4 \cdot e_{tot}$	-	0.63	-	0.96	0.97	0.99
***Rot*@ F_5=50**	-	15.7	-	60.2	2.56	23.5
$F_5 \cdot e_{tot}$	-	1.12	-	1.85	1.58	1.2

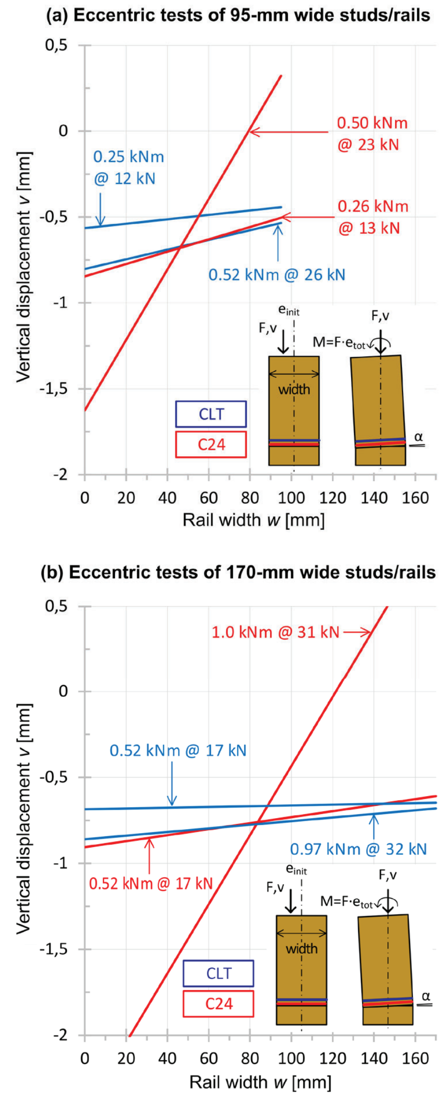

Figure 6: Displacement plotted over the stud width for (a) 95- and (b) 170-mm wide studs and during different loading stages selected to enable comparison.

displacements to calculate the angle α, are taken from the markers attached to the stud, see Fig. 2. In the figure, load stages recorded by the DIC- system closest to moments M_i = 0.25, 0.5 and 1.0 kNm are selected and shown. Since the eccentricity e_{tot} varies between setups these moments occur at different vertical loads F_i, which are also indicated in the figure. The results clearly show that the CLT- rail causes significantly less rotation and vertical displacement than the C24 rail. The difference is mostly relevant in situations where high rotational stiffness is desirable, for instance to avoid large deformations at the supports in a buckling design.

4.3 FAILURE MODES

During the tests, significant interpenetration was observed between the CLT layers 2 and 4 and studs in the contact zone, see Fig. 7 (a-b). This behaviour resulted in saw teeth profiles caused by interpenetrations between the annual rings of the wood materials where strong latewood bands pushed into earlywood areas. For the C24 rails and CLT layers 1, 3 and 5, the penetration/crushing mainly occurred in the rails with local fracture at the contours of the studs as shown also in the photographs. In addition, as a secondary failure type, shear fracture in studs, occurred when vertical displacements were large as shown in Fig. 7 (c-d). The cracks initiated at boundaries between 0° and 90° layers — no fracture occurred at the interface of layers in the CLT rails — and propagate along the stud fibre directions. Despite significant crack opening happened, the force F did not drop.

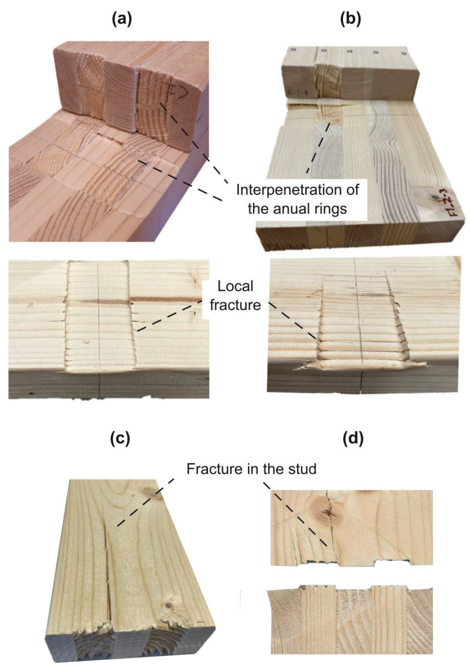

Figure 7: *Photographs of the penetration failure at contact zone for both (a) centric and (b) eccentric tests as well as (c-d) the fracture in the studs for large vertical displacements.*

4.4 FE MODEL CALIBRATION

For the simulations of centric tests, the outputs of the calibrated models are shown in black dashed lines overlapped with experimental data in Fig. 4 (a-b). For the 95-mm configurations, the normal contact stiffness 0°/90° of 175 N/mm^3 was found first using the C24 rail tests. Then, the normal contact stiffness 0°/0° of 200 N/mm^3 was calibrated using CLT rail tests. Likewise, for 170-mm wide configurations, the normal contact stiffness 0°/90° was 175 N/mm^3 and the normal contact stiffness 0°/0° was 350 N/mm^3.

The calibrated contact stiffnesses were used for simulating the eccentric tests, see black dashed lines in Fig. 5 (a-b). For those simulations, the slope parameter in Eq. (1) was determined as $a_{\text{CLT.95}}$ = 11.3 for the 95-mm wide CLT configuration and $a_{\text{C24.95}}$ = 9.2 for the 95-mm wide C24 configuration. For the wider configurations it was determined as $a_{\text{CLT.170}}$ = 10 and $a_{\text{C24.170}}$ = 4.9 respectively. The coupled displacements onset v_e = 0.3 mm was the same for all eccentric simulations.

4.5 COMPLIANCE IN THE TESTED SPECIMENS

Here, the objective is to illustrate the contribution of each section in the stud-rail systems to the global compliance. The main outcomes are shown in the Fig. 8 where the calculated nodal vertical displacements from the centrally loaded FE models are plotted along the vertical axis. The nodal displacements are normalized by the maximum value at F = 10 kN for all four setups. For the C24 rails, it has typically more deformation are observed in the rails while this deformation is considerably reduced in the CLT rails. From the top, dz1 displaces more than dz 2— except for 170-mm C24 rails where dz2 behaves similar to dz1. In the contact zones, the flat region in the graph corresponds to the penetration in the CLT rails, which is less apparent for the C24 specimens.

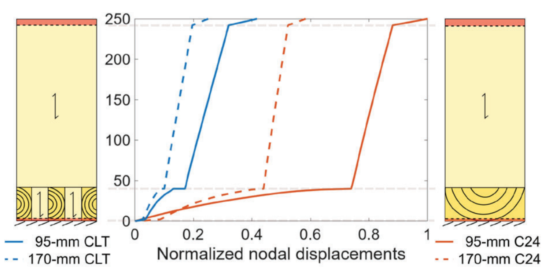

Figure 8: *Normalized nodal displacements along the stud-rails from the centric FE models.*

5 – FE PARAMETRIC STUDIES

5.1 GLOBAL EFFECT OF CONTACT STIFFNESS

The relatively good calibration of the FE models has been achieved because of the use of contact stiffnesses as the tuning parameters. It is also interesting to understand how those parameters affect the global behavior of the

https://doi.org/10.52202/080513-0606

stud-rail structural members. Fig. 9 shows the force F versus the vertical displacement at the plate on top the stud to present the sensitive of the contact stiffnesses in the FE models. Both models were computed in the centric load case. The perpendicular contact stiffness $K_{\mathrm{contact},0°/90°}$, computed from the C24 FE models, has shown to have negligible influence in the global stiffness as shown in Fig. 9 (a-b). This is not surprising since the deformations in the contact zone is marginal compared to the deformations in the rail, see Figure 8. The stiffness was evaluated in 4 different sets from the calibrated ones, including a case without any penetration computed with the hard-contact penalty numerical approach in Abaqus represented by infinity symbol. On the contrary, computed from the CLT FE models, the parallel contact stiffness $K_{\mathrm{contact},0°/0°}$ notably affects the force-displacement relation. For example, for the 95-mm wide models, the global stiffness increases by approximately 10% compared to the calibrated value when $K_{\mathrm{contact},0°/0°}$ is doubled and decreases with 20% when $K_{\mathrm{contact},0°/0°}$ is halved. A similar trend is seen in the 170-mm wide models, but effects are slightly smaller. The reason for this could be that the ratio of effective contact area for the 95-mm wide model $A_{\mathrm{layers\ 2\ and\ 4}}/A_{\mathrm{stud}}$ = 0.43 is higher than of the 170-mm wide models $A_{\mathrm{layers\ 2\ and\ 4}}/A_{\mathrm{stud}}$ = 0.35.

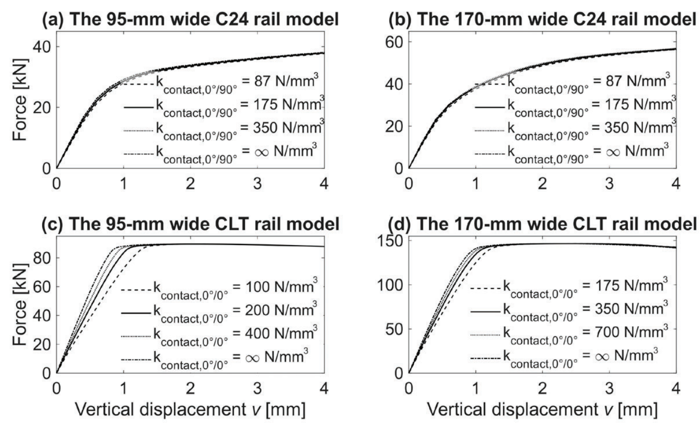

Figure 9*: Parametric studies of different normal contact stiffnesses in (a-b) perpendicular interaction $K_{contact,0°/90°}$ and (c-d) parallel interaction $K_{contact,0°/0°}$.*

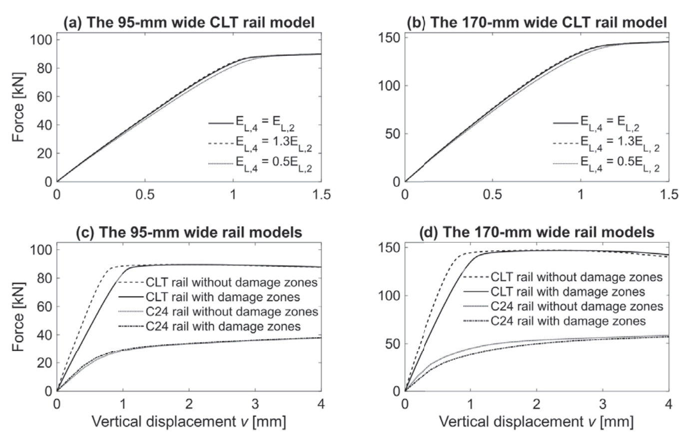

Figure 10*: Parametric studies of different (a-b) longitudinal elastic modulus in the CLT layer 4 and (c-d) the effect of damage zones in the models.*

5.2 GLOBAL EFFECT OF VARIATION IN MECHANICAL PROPERTIES: CLT LAYERS AND DAMAGE ZONES

From dynamic modal tests, see Appendix A.1, one observation was that elastic properties vary between CLT layers 2 and 4, in particular the longitudinal elastic modulus. Fig. 10 (a-b) therefore shows simulations carried out with fixed E_L in the CLT layer 2 while varying values in the CLT layer 4. For both the 95-mm wide and 170-mm wide models, the global stiffness has not changed considerably as shown in Fig. 10 (a-b). However, the stresses change; Stress analysis in the stud-CLT rail systems is convenient to further investigate and the developed FE models can be explored in this regard, but it goes beyond the scope of this paper.

Another particular aspect in the models, which is seldom considered in wood structures, is the damage zones. To investigate the effect of those, Fig. 10 (c-d) shows the global force-displacement curves from simulations with and without damage zones. For the C24 configurations, the effect of damage zones is smaller for the 95-mm wide model than the 170-mm wide model. However, for the CLT models, this significantly reduces the global stiffness, lowering it by approximately 25 % for both rail sizes. In general, the damage zones have a more pronounced effect on the CLT models compared to the C24 models. This is in line with the results presented in Figure 8 where the deformations in the damage zones are very small compared to the compression of the C24-rail

6 – CONCLUSION

A CLT rails of two different cross section dimensions were tested in centric and eccentric compression tests and compared to behaviour observed in their counterparts made of C24 structural timber. FE models were developed and validated for assessing the global mechanical behavior of the structures. The main conclusions are:

- CLT rails have approximately 2 times higher maximum loading-bearing capacity than C24 rails.
- The stiffness of CLT rails is about 2-3 times higher than that of C24 rails while loading centrically.
- At the buckling load for a typical 45 × 95 mm stud around the strong axis, the rotation is 3 times larger for the C24 rail system than for CLT rails systems for an eccentric load case.
- Significant fiber-fiber penetrations between studs and CLT-rails were observed leaving permanent indentations in the timber material.
- Crack in the studs were observed while compressing the CLT stud. Those cracks that happened at large vertical displacements should be investigated as they might lead to structural instabilities.
- Implementation of an over-closure pressure contact strategy within the FE model demonstrated a useful approach to compensate for local penetration phenomena. The calibrated FE models accurately simulates global stiffness and local displacements at the DIC markers.
- Parametric studies shows that normal contact stiffnesses $K_{\mathrm{contact},0°/0°}$ (layers 2 and 4) influence the global behavior of the CLT-rail, but for the relatively soft C24-rail the contact stiffness $K_{\mathrm{contact},0°/90°}$ has a negligible influence.
- Parametric studies shows that the difference in longitudinal moduli in different the CLT layers 2 and 4 does not affect the global stiffness much.
- Parametric studies revealed that the damage zones significantly impacted the global stiffness of CLT configurations but had minimal effect on C24 configurations for which the compression of the rail dominates.

Overall, the work has shown superior loading-bearing capacity of CLT rails from re-used cut-outs over its counterpart made of C24 structural timber. The reported structural relations, such as force-displacement relation, force-rotation and contact stiffnesses, are relevant and can later be used to develop simple structural elements to be integrated into more complex models of full-scale timber structures such as prefabricated timber modules.

ACKNOWLEDGMENTS

Stora Enso is acknowledged for supplying the materials. The authors are grateful for the research funding from the Knowledge Foundation (KKS), KK project number 20210063. Eng. Lars Pettersson, Eng. Emil Lockner and Eng. Edvard Henriksson are acknowledged for their assistance in the experimental tests.

REFERENCES

[1] R. Maharjan, L. Kuai, J. Vessby, S. Ormarsson. “An experimental analysis of full-scale light-frame timber modules.” Engineering Structures 304 (2024), 117617.

[2] J. Vessby, M. Perstorper, F. DeMonte, and J. Eriksson. “Structural use of cut-offs from CLT-production – three examples that utilize the unique properties.” World Conference on Timber Engineering, Oslo, Norway, 2023.

[3] ETA-14/0349. “European Technical Approval for Cross Laminated Timber.” Stora Enso Wood Products, 2020.

[4] EN 408:2010+A1:2012 - Determination of some physical and mechanical properties.

[5] M. Totsuka, R. Jockwer, H. Kawahara, K. Aoki, M. Inayama. “Experimental study of compressive properties

https://doi.org/10.52202/080513-0606

parallel to grain of glulam." Journal of Wood Science (2022) 68:33.

[6] M. Totsuka, R. Jockwer, K. Aoki, M. Inayama. "Compressive stiffness parallel to grain in timber." World Conference on Timber Engineering, Oslo, Norway, 2023.

[7] J.R. Airaa, F. Arriaga, G. Íñiguez-González, J. Crespo. "Static and kinetic friction coefficients of Scots pine (Pinus sylvestris L.), parallel and perpendicular to grain direction." Materiales de Construcción, 64 (2014) 315.

[8] S. Akter, E. Serrano, T. Bader. "Numerical modelling of wood under combined loading of compression perpendicular to the grain and rolling shear." Engineering Structures 244 (2021) 112.

[9] R. F. S. Hearmon. "Theory of the vibration testing of wood." Forest Products Journal 16 (1966), pp. 29-40.

[10] M. Perstorper, J. Vessby, and E. Lockner. "Bending properties of 100 narrow CLT-based boards – static and dynamic tests and DIC analysis." World Conference on Timber Engineering, Oslo, Norway, 2023.

[11] E. Lockner. "En jämförelse av stämpeltryck på syllar av korslimmat trä och av konstruktionsvirke" (In Swedish), Karlstad University, 2020.

[12] E. Henriksson. "Rotationsstyvhet i syllar av korslimmat trä och konstruktionsvirke vid excentrisk last" (In Swedish), Karlstad University, 2023.

APPENDIX A.1 ELASTIC PROPERTIES OF THE RAILS AND STUDS

The longitudinal elastic moduli E_L, and shear moduli G_{LR} and G_{LT} were experimentally determined via dynamic modal tests [10].

Small clear samples (10×10 mm) with a length in the fibre direction of approximately 40 mm were cut from neighboring CLT-boards that had the same lamella material in layer 2 and 4 as the CLT-rails tested. For the C24 material, similar samples were cut from radial strips, see Fig. A1(a). The tested C24 boards were supplied with different sizes of growth rings depicted also in Fig. A1 (a) and therefore the measured properties here are related to the average of them all.

The longitudinal modulus of elasticity E_L was determined based on axial (lengthwise) vibrations from a hammer excitation captured by a high-frequency microphone using Eq. A1 for free-free boundary conditions.

$$E_L = 4(f_{A-1}L)^2\rho \qquad \text{(A1)}$$

where $f_{A\text{-}1}$ is the fundamental axial resonance frequency (Hz), ρ is the measured density (kg/m^3) and L is the sample length (m). The shear modulus was determined from free-free torsional vibration using Eq. A2 and represents a mixture of G_{RL} and G_{TL}. They are therefore assigned the same value equal $G_{T\text{-}1}$.

$$G_{T-1} = (f_{T-1}2L)^2\rho\frac{I_p}{K_t} \qquad \text{(A2)}$$

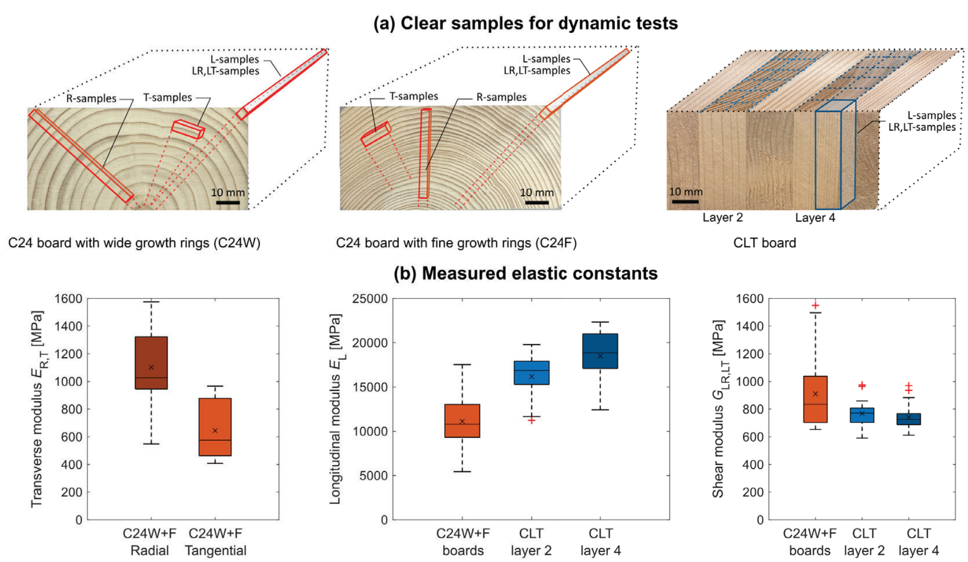

***Figure A1**: (a) Locations of the small clear samples cut from C24 boards as well as for the CLT layers 2 and 4 by the dynamic modal tests. (b) The box plots of the elastic constants: longitudinal E_L and transverse $E_{R,T}$ moduli, and shear modulus $G_{RL,TL}$.*

where $f_{T\text{-}1}$ is the fundamental torsional resonance frequency (Hz), I_p = polar moment of inertia (m^4) and K_t is the torsional constant (m^4).

The transverse elastic moduli E_R and E_T were measured in the same way as the E_L on specimens taken from the C24-material. Radial specimens were appr. 4×4 mm with a length of 30-45 mm. The small tangential width ensured minimal influence of ring curvature. Tangential specimens were shorter (L= 15-25 mm) to avoid influence of ring curvature The remaining elastic constants such as the shear modulus G_{RT}, and the Poisson rations ν_{RT}, ν_{RL} and ν_{TL} were taken from the literature [9]. All values are tabulated in Table 1 as mean values for the CLT rails and C24 studs.

APPENDIX A.2 DAMAGE ZONES: SIZE AND FICTICIOUS ELAST MODULUS

In this study, some studs in the compression tests were speckled using white and a black spray paint at one test for each centric configuration to measure the compressive strain enabling to estimate the size of dz1. In this regard, the outcome related to damage zone size were rather similar for both 95-wide and 170-wide configurations and therefore this section only presents strains of 95-wide configurations. The strain component ε_y in the studs were analysed from five lines along the studs positioned in the centre of each CLT layer as illustrated in the bottom of Fig. A2 (dashed lines). The overlapping of strains along the lines were plotted at three force levels for the CLT (a, c and e) and C24 (b, d and f) rail configuration, see Fig. A2. At relatively low force levels in (a) and (b), higher strains were found near dz1 and the contact between stud and rail while the strains within the stud were close to zero. By increasing the forces, the compressive strains change only in dz1 while the strains within the stud are still small except at some local positions were higher strains where found caused by local effects (e.g., at 50 mm above the contact in (c) and (d)) attributed to knots. The trend when increasing the force is increasing in magnitude of strains in dz1. The strains near the stud-to-rail contact zone do not exhibit a clear trend because of the considerable penetration within that contact zone.

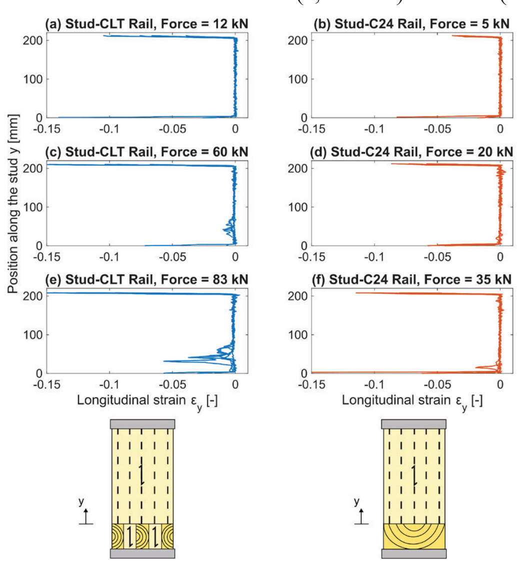

Figure A2: *Longitudinal strain distribution in the studs at different force levels for CLT and C24 rail configurations.*

In this study the size of the dz1 was about 8 mm measured from Fig. A2(a-b). This aligns with previously reported values for unplanned spruce (≈ 1-10 mm) [5-6]. The size of dz2 was estimated as 2 mm evaluated where the studs were positioned at ends of rails so that field could be computed in the rails. Those were analyzed similarly as in [11-12]. The smaller size in the bottom is because of planning process. Totsuka et al. [5] also found that planned wood (Cedar and Cypress) had smaller size of the disturbed zones (≈ 2 mm) compared to unplanned spruce.

The elastic moduli of damage zones were calibrated with the FE models using the markers. In this calibration, the variation of average distance between the markers and plate 2 *dl* from the centric tests were assessed and plotted against the sampled forces (see Fig. A3). As a result, the fictitious elastic moduli of the dz1 were found to be about 6 % of the "real" moduli measured in the stud ($E_{L,dz1}/E_{L,stud} = 0.06$). Totsuka et al. [6] reported this difference to be 1-4 percent. The difference between the studies is relatively small, but it is worth mentioning the scatter in elastic properties in the studs, caused for instance by reaction wood. In addition, for all simulations in this work, the six-percent fictious modulus was considered for both damage zones.

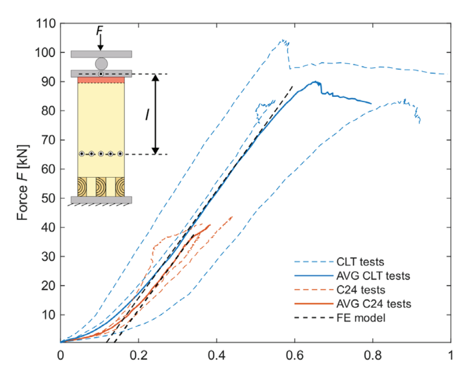

Figure A3: *Calibration of fictitious elastic moduli in the dz 1.*

https://doi.org/10.52202/080513-0606